Letter

Thermal conductivity of monolayer graphene: Convergent and lower than diamond

Zherui Han and Xiulin Ruan*

School of Mechanical Engineering and the Birck Nanotechnology Center, Purdue University, West Lafayette, Indiana 47907-2088, USA

(Received 1 March 2023; accepted 14 September 2023; published 29 September 2023)

The thermal conductivity of monolayer graphene is widely believed to surpass that of diamond even for few-micron-size samples and was proposed to diverge with system size. Here, we predict the thermal conductivity from first principles by considering four-phonon scattering, phonon renormalization, an exact solution to the phonon Boltzmann transport equation (BTE), and a dense enough sampling grid. We show that at room temperature, the thermal conductivity saturates at 10 μm system size and converges to 1300 W/(m K), which is lower than that of diamond. This indicates that four-phonon scattering overall contributes 57% to the total thermal resistance and becomes the leading phonon scattering mechanism over three-phonon scattering. On the contrary, considering three-phonon scattering only yields higher-than-diamond values and divergence with size due to the momentum-conserving normal processes of flexural phonons.

DOI: 10.1103/PhysRevB.108.L121412

Graphene is a subject of extensive research due to its unique properties and observed exotic transport phenomena [1–6]. Among them, many experimental and theoretical studies have shown that the thermal conductivity (κ) of graphene surpasses that of diamond, even for small samples of few-micron size [7–11], and some suggest that it diverges with the system size [12]. Several other experiments reported lower thermal conductivity values, which were commonly attributed to defects and impurities [13–15]. Moreover, the uncertainty of these measurements is usually too large to conclusively assess whether or not κ is higher than that of diamond. Sources of uncertainty include optical absorption [13], strong nonequilibrium among different phonon modes [16,17], and others.

The studies of thermal transport in graphene have yielded several new insights associated with two-dimensional (2D) materials, supporting graphene's high and divergent thermal conductivity. By coupling the linearized phonon Boltzmann transport equation (BTE) with empirical potential [8] or first principles [9] at the three-phonon (3ph) level, it was found that the flexural phonons (ZA) [18] contribute significantly to κ and their 3ph scattering is greatly suppressed by a selection rule [8]. Due to strong momentum-conserving scattering (normal process), thermal conductivity did not converge for a system size of 50 μm, and the value for the 10 μm size with boundary scattering at room temperature [∼3000 W/(m K)] is in accordance with another theoretical study at the 3ph level [10] that reports ∼2500 W/(m K) for a 10 μm sample. On the other hand, while acknowledging the out-of-plane vibrations, it has been proposed [12] that graphene resembles a 2D nonlinear lattice that was extended from the Fermi-Pasta-Ulam-Tsingou (FPUT) model [19]. Therefore, the heat transport is non-Fourier [20] and κ should diverge with system size as $\kappa_{2D} \propto \log_{10}(L)$ [21,22].

However, questions were recently raised regarding whether these insights represent the complete physics of thermal transport in graphene. In particular, can higher-order phonon scattering be neglected in graphene, considering that the 3ph scattering is restricted in graphene and four-phonon (4ph) scattering has been found to be important in other solids [23–26]? Also, is it sufficient to explain the behavior of graphene in terms of the 2D lattice model considering that it is actually only a quasi-2D system with out-of-plane atomic vibrations? To answer these questions, Feng and Ruan [27] computed 4ph scattering rates with empirical potential and showed a strong 4ph effect in the ZA mode and, consequently, obtained a system size convergent and greatly reduced κ of around 800 W/(m K). The sampling grid that was accessible there was relatively coarse. Gu *et al.* further incorporated phonon renormalization into this calculation with empirical potential and argued that ZA scattering rates are reduced by temperature modification [28]. However, the empirical interatomic potentials used in these studies do not accurately represent chemical bonds, and the exact role of four-phonon scattering and the value of κ remain elusive. Another mainstream approach is molecular dynamics (MD), with two different flavors in equilibrium (EMD) and nonequilibrium (NEMD) treatments. In theory, the MD approach is expected to capture all orders of anharmonicity. However, the EMD simulations show size-converged κ ranging from 1000 to 2000 W/(m K) [29–31], while the NEMD simulations show logarithm length dependence up to several microns [12,32]. Interestingly, one MD study presents a saturation of κ when L is extended to 100 μm [33]. Besides these inconsistencies, MD simulations also suffer from the classical phonon statistics and empirical potentials; hence, the results can only be interpreted qualitatively.

Summarizing all existing studies, the thermal conductivity of pristine suspended monolayer graphene is currently widely perceived, both experimentally and theoretically, to be around 3000 W/(m K), even for samples of few-micron

*ruan@purdue.edu

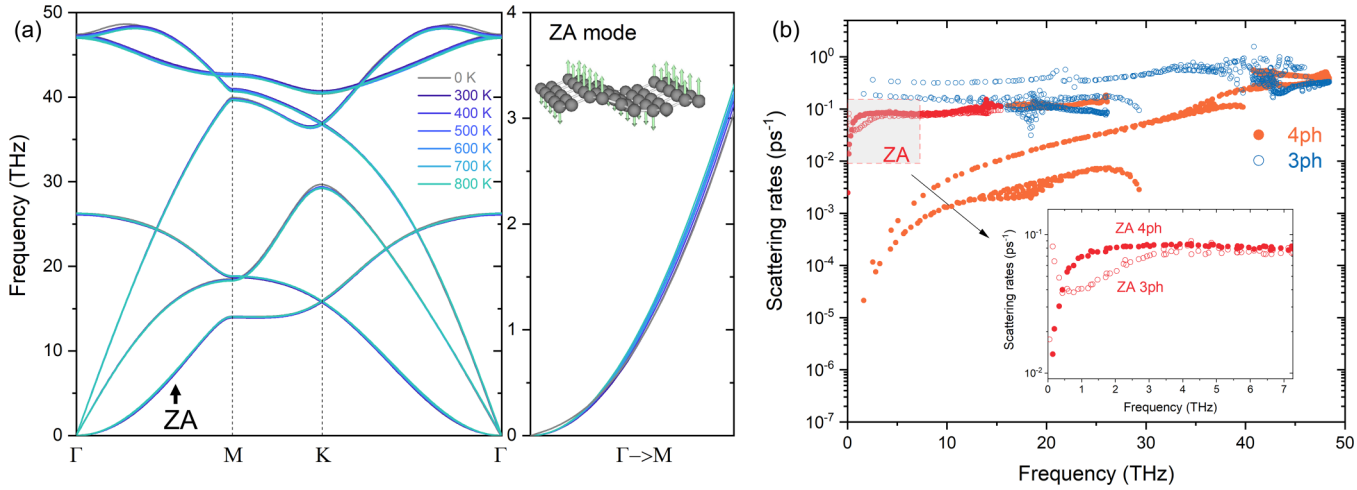

FIG. 1. Phonon self-energy in graphene. (a) Phonon dispersion at finite temperatures by the TDEP method. Dispersion at 0 K is obtained by density functional perturbation theory. The right panel is a zoom-in plot of the ZA mode dispersion from Γ to M in the Brillouin zone. The schematic of ZA out-of-plane vibrations is created by an online visualization tool [34]. (b) Spectral phonon scattering rates at 300 K. The scattering rate in the y axis is presented in logarithm scale. Three-phonon ($\tau_{3\text{ph}}^{-1}$) and four-phonon ($\tau_{4\text{ph}}^{-1}$) scattering rates are shown as hollow and filled circles, respectively. The scattering rates of the ZA mode are marked in red and zoomed-in in the inset.

size and higher than that of diamond and graphite. On the other hand, the lower values, as seen in some other experiments and simulations, were thought to be due to defects or impurities, or considered as inconclusive due to large uncertainty in the experiments and inaccuracies in the simulations. In this Letter, we revisit the thermal conductivity of graphene with first-principles-computed four-phonon scattering, phonon renormalization, an exact solution to the phonon Boltzmann transport equation (BTE), and a dense enough sampling grid. We show that the thermal conductivity, contrary to popular perception, saturates at 10 μm and converges at a room temperature value of 1300 W/(m K), which is lower than that of diamond. This represents a factor of 2.31 reduction from 3000 W/(m K) and indicates that four-phonon scattering becomes the leading phonon scattering mechanism. The considerations of both four-phonon scattering [23,24] and phonon renormalization [35–38], which form the unified approach [39,40], have successfully explained the Raman linewidth of suspended graphene in our prior work [41]. Here, we extend the methodology to all phonon modes for thermal conductivity prediction. The phonon BTE is exactly solved by an iterative scheme [42] incorporating both three-phonon and four-phonon scattering after we manage to store the iterative processes within one terabyte memory space accessible in modern supercomputer architecture. We compute, from first principles, that the ZA mode has strong four-phonon scattering rates which are comparable to their three-phonon counterpart. The sampling grid (q mesh) is carefully checked for κ convergence of an infinitely long graphene sample and we see convergence of thermal conductivity after including four-phonon scattering ($\kappa_{3\text{ph}+4\text{ph}}$), but not with three-phonon scattering ($\kappa_{3\text{ph}}$) only. Our findings challenge the perception of graphene being a better heat conductor than diamond, and will motivate future experimental validation efforts.

Our first-principles calculations are based on density functional theory as implemented in the VASP package [43]. The phonon renormalization effect is included by a temperature-dependent effective potential (TDEP) method [36] to compute temperature-dependent phonon dispersions and interatomic force constants (IFCs) [38]. Phonon scattering rates, summed up by Matthiessen's rule [44] $\tau_\lambda^{-1} = \tau_{\lambda,3\text{ph}}^{-1} + \tau_{\lambda,4\text{ph}}^{-1} + \tau_{\lambda,\text{iso}}^{-1}$, are computed by our FOURPHONON code [45], an extension module to the SHENGBTE package [46]. The exact solution of the BTE is implemented in the same solver by a shared-memory parallel computing strategy [47].

The computed phonon dispersion and phonon scattering rates are presented in Figs. 1(a) and 1(b), respectively. Overall, graphene is quite rigid, as shown by the very small change of phonon frequency at finite temperatures [see Fig. 1(a)]. The frequency of in-plane optical phonons decreases with increasing temperature, a signature that has been analyzed and experimentally verified in our prior work [41]. Contrary to the decreasing trend of frequency shift for in-plane optical phonons, we find that the flexural phonons are hardened with rising temperature [see Fig. 1(a), right panel]. This is a result of the coupling between flexural phonons and in-plane degrees of freedom in freestanding graphene [18]. Renormalized flexural phonons do not have a strictly quadratic dispersion. With the renormalized phonon dispersion and temperature-dependent IFCs, one can then compute the spectral phonon scattering rates τ_λ^{-1} using Fermi's golden rule, as shown in Fig. 1(b). Interestingly, the optical phonons and flexural phonons show comparable or even higher four-phonon scattering rates ($\tau_{4\text{ph}}^{-1}$) with their three-phonon counterpart ($\tau_{3\text{ph}}^{-1}$), while the rest of the phonon modes are dominated by three-phonon scattering. Optical phonons having large $\tau_{4\text{ph}}^{-1}$ are understood as they easily satisfy the energy conservation in the recombination scattering events: $\lambda_1 + \lambda_2 \rightarrow \lambda_3 + \lambda_4$ [48]. On a different ground, the reason for the flexural phonons lies in the selection rule for general quasi-2D systems [8] in which only even numbers of flexural phonons can be involved in a phonon scattering event due to reflection symmetry. As a result, the phase space for three-phonon scattering is much smaller than that of four-phonon scattering [27]. The ZA

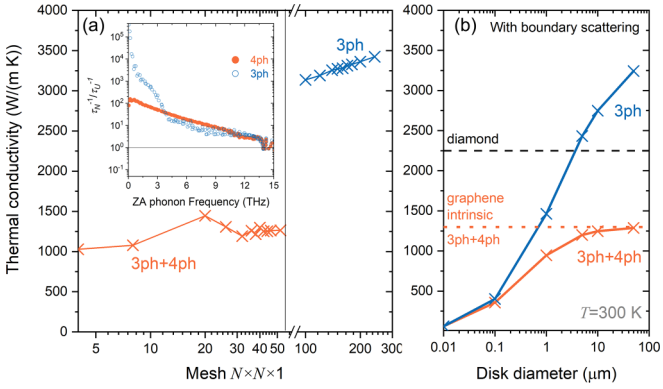

FIG. 2. Convergence of thermal conductivity of graphene at room temperature. (a) Convergence with respect to mesh size without boundary scattering. Mesh size in the x axis is presented in logarithm scale. The inset shows the ratio of ZA mode scattering rates from normal (τ_N^{-1}) and Umklapp (τ_U^{-1}) processes for both 3ph (hollow blue dots) and 4ph channels (filled orange dots). (b) Size-dependent thermal conductivity with boundary scattering under 3ph and 3ph+4ph theories.

mode was considered as the major heat carrier in graphene under the 3ph scattering picture [8,9,49]; this statement needs to be reexamined after its strong $\tau_{4\text{ph}}^{-1}$ is included.

We next solve for the intrinsic thermal conductivity by an iterative scheme [42] to account for the collective phonon excitations. This approach distinguishes the normal processes (N) that are momentum conserving and Umklapp processes (U) that are resistive. Such a treatment is important for graphene since it has a strong normal scattering process associated with its phonon hydrodynamics nature [50,51]. The coupled equations are presented in the Supplemental Material [52]. For the BTE solution to generate meaningful results, one has to check the convergence of κ with respect to the sampling grid in the Brillouin zone (q mesh). An infinitely large system has finite thermal conductivity if a convergence can be reached. Figure 2 shows our test of convergence when 3ph or 3ph+4ph is included in the calculations. Mesh size $N \times N \times 1$ is uniform in-plane. In all these calculations, the energy broadening factor is unity to ensure the accuracy within our computational power. We find that with four-phonon scattering, $\kappa_{3\text{ph}+4\text{ph}}$ converges around a mesh size of $N = 40$, and further increasing the mesh to $N = 52$ does not change the value of κ. In contrast, $\kappa_{3\text{ph}}$ does not reach convergence up to $N = 240$ and scales logarithmically with mesh size N. Note that the prior work [10] used $N = 128$ for 3ph. To illustrate the impact on practical samples of finite size, we plot the size-dependent thermal conductivity in Fig. 2(b) by adding a boundary scattering term [9,10]: $\tau_{\lambda,b}^{-1} = |\mathbf{v}_\lambda|/L$, where $\mathbf{v}_\lambda$ is the group velocity of phonon mode λ and L is the disk diameter. The 3ph and 3ph+4ph results start to show a considerable difference when the size is larger than 0.1 μm. At the 3ph+4ph level, κ would reach the intrinsic limit at around 10 μm, while the 3ph curve does not converge even for 50 μm. To inspect the origin of this behavior, we decompose the N/U scattering for the ZA mode and plot the ratio of two types of scattering events, τ_N^{-1}/τ_U^{-1}, in the inset of Fig. 2(a). Apart from the dominant role of the normal process for both scattering channels, it is, to a lesser degree, for four-phonon scattering of flexural phonons at low frequencies. Given the fact that τ_N^{-1} decreases when $\omega \to 0$, we conclude that 3ph of long-wavelength flexural phonons is almost entirely contributed by normal processes. The extreme case is the heat conduction in a 2D nonlinear lattice, where all scattering processes are momentum conserving [22] and the thermal conductivity is logarithmic divergent. Thus, we explain the finite intrinsic thermal conductivity of graphene from two related arguments: (i) four-phonon scattering provides an additional scattering channel; (ii) for long-wavelength phonons, four-phonon scattering has a considerable number of resistive U scattering events, but three-phonon processes are nearly all N scattering events, implying a divergence. Our numerical results share similarities with a theoretical work on a carbon nanotube (CNT) [53], where the authors estimated that third-order anharmonicity leads to a divergence of thermal conductivity due to vanishing scattering of long-wavelength phonons. They empirically showed that a higher-order process can remove such divergence. While the study on CNT is worth further investigations [54–56], we show here that four-phonon scattering converges the thermal conductivity of graphene from first principles.

The above arguments can further be seen in the spectral κ [Fig. 3(a)], where we find a singularity for near-zero frequency phonons at the 3ph level, but not at the 4ph level. The 3ph and 3ph+4ph pictures have a distinct spectral trend for low-frequency phonons. While the 3ph+4ph calculation can saturate the spectral κ when $\omega \to 0$, the 3ph-only calculation shows an up-soaring spectral trend. In addition, we analyze the ZA mode contribution to κ, as shown in Fig. 3(b). At the 3ph level with $N = 180$, the ZA contribution is 2833 W/(m K) and 85%. After including 4ph scattering, the ZA contribution becomes 949 W/(m K) and the percentage reduces to 73% for intrinsic graphene. The argument that ZA modes are the major heat carriers in graphene [8,9] still holds. Note that our first-principles result is different from previous MD work [29]. Despite the fact that MD gives a total κ around 1000 W/(m K), it estimates the ZA mode contribution to be only one-third of total κ. This could be due to the classical statistics that overpopulates the non-ZA phonon branches.

Finally, we present the calculated thermal conductivity of graphene as a function of temperature and some comparisons to other carbon allotropes in Fig. 4. Our results κ_L at the 3ph level for 10-μm-size graphene with boundary scattering are consistent with prior first-principles studies [9,10] and we see a small impact from phonon renormalization (see Supplemental Material [52] for a comparison without renormalization). The comparison in Fig. 4(a) shows that incorporating 4ph in the calculation significantly reduces $\kappa_{3\text{ph}}$. Nevertheless, our results of $\kappa_{3\text{ph}+4\text{ph}}$ are significantly higher than the previous simulation with empirical potential at moderate mesh size [27]. This indicates that the optimized Tersoff potential probably overestimates the fourth-order anharmonicity of the ZA phonons. At room temperature and without boundary scattering, we predict that $\kappa_{3\text{ph}+4\text{ph}} = 1298$ W/(m K). This represents a factor of 2.31 reduction from 3000 W/(m K) and indicates that 4ph scattering overall contributes 57% to the total thermal resistance and becomes the leading phonon scattering mechanism over 3ph scattering. As a

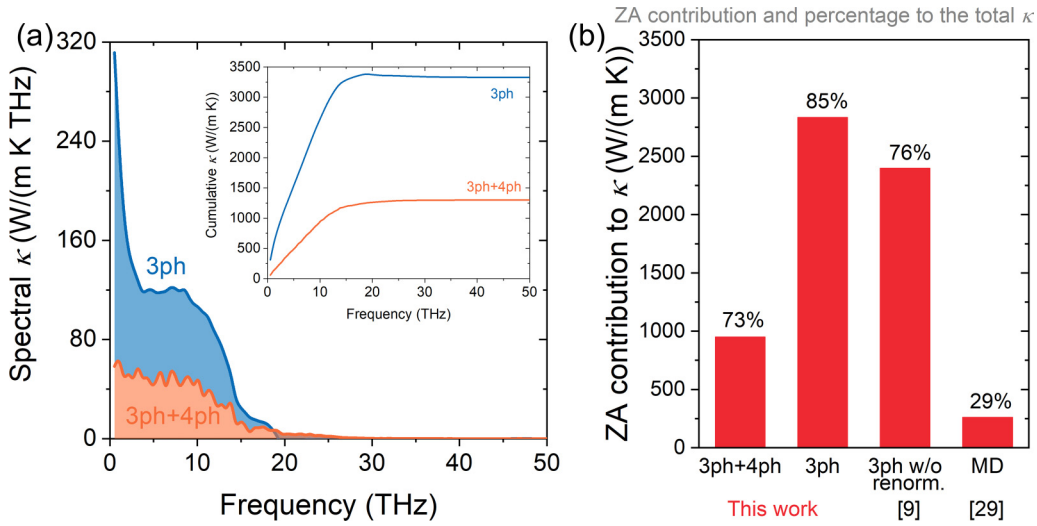

FIG. 3. Spectral and mode contribution. (a) Spectral contributions to κ of graphene at room temperature without boundary scattering. The inset shows the cumulative thermal conductivity as a function of phonon frequency. (b) ZA phonons' contribution to κ and its percentage at room temperature, and comparison to first principles at 3ph (renorm. stands for phonon renormalization that was not included before) [9] and MD work [29]. In both plots, the 3ph case presented here is calculated at $N = 180$ without boundary scattering, and note that it is not converged with N.

result, the thermal conductivity of graphene is lower than that of diamond from 300 to 800 K. The first-principles results for diamond [green and black lines in Fig. 4(a)] are from Refs. [24,39], where similar methodologies were applied, including 3ph/4ph scattering, phonon renormalization, and iterative solution to BTE. The comparisons show that both 4ph scattering and the phonon renormalization effect are not significant in diamond. Note that the thermal conductivity of diamond is well received, with good agreements between simulations and experiments [57–59,62]. In contrast,

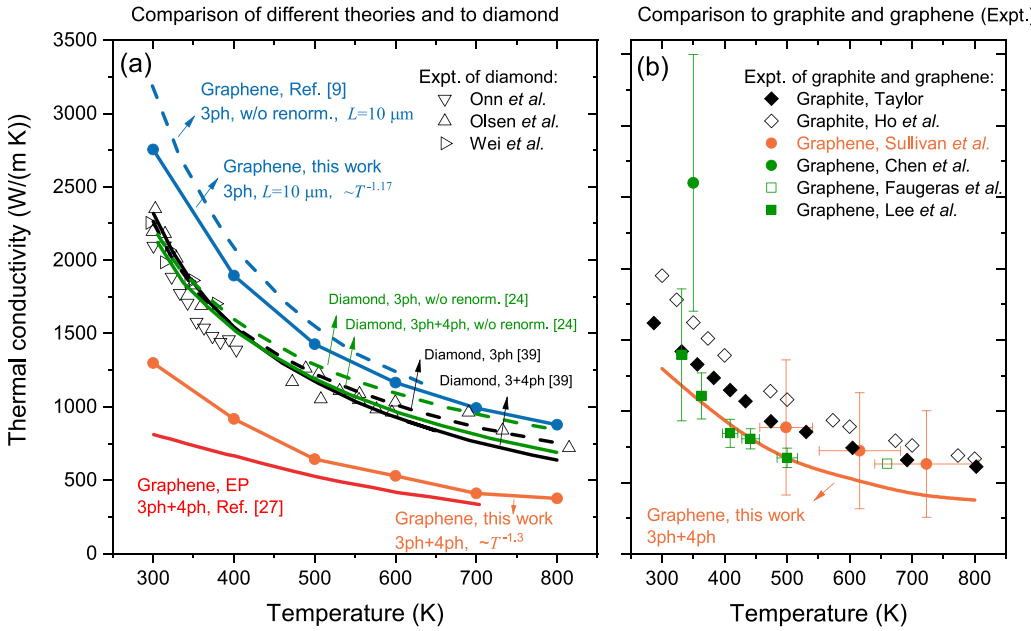

FIG. 4. Thermal conductivity of graphene as a function of temperature. (a) Prior theoretical work with empirical potential (EP) and four-phonon scattering [27] is presented as a red solid line. Our results are presented in connected solid lines with orange (3ph+4ph) and blue (3ph scattering only and a boundary scattering of $L = 10\,\mu$m). Also, a prior first-principles 3ph work with boundary scattering [9] is shown as a dashed blue line. Computational results for diamond without renormalization [24] and with renormalization [39] are presented in green and black lines, respectively (3ph results in dashed lines and 3ph+4ph results in solid lines). Several experiments on diamond are also plotted here (right-pointing triangles [57], triangles [58], inverted triangles [59]). (b) Our results compared to a recent Raman measurement on suspended graphene [17] (filled orange circles) and other previous Raman measurements (green filled circles [13], open squares [14], filled squares [15]), and experiments on graphite [60,61] (black diamonds).

the measured thermal conductivity values of graphene so far have shown a large spread. While our finding challenges a popular perception that graphene is a better heat conductor than diamond, the numerical results are self-consistent with advancements in theories and computational power. Under current computational formalism, a plausible reason for this observation is that diamond does not have strong four-phonon scattering for acoustic modes [24,39], but flexural phonons in graphene do have large four-phonon scattering rates originated from its 2D nature. In this sense, the reduction of κ from diamond to graphene is understandable. Interestingly, the comparison between diamond and graphene singles out the effect of the dimensionality, which contributes through flexural phonons. Going from a 3D (bulk) to quasi-2D case, one of the transverse acoustic vibrations shifts from a linear to a quadratic dispersion relation and its 3ph scattering is restricted by the selection rule, while 4ph scattering becomes significant. Also, because of this selection rule, the fifth-order term as an odd term should also be restricted. Since the higher-order term generally has smaller coupling matrices, we also expect the sixth-order term and all other even-order terms to be negligible for the case of graphene.

In Fig. 4(b), we also cautiously compare our results to a recent Raman measurement on a suspended graphene sample (in orange) [17] that is based on the apparent phonon temperature, and show the estimated κ from previous Raman measurements (in green) [13–15]. Large spread and uncertainty of the measured data are observed. It should be noted that some experimental data in Fig. 4(b) appear to agree with our results in a certain temperature range. However, they cannot be considered as having supported our prediction over the entire temperature range yet because the uncertainty is too large to draw a conclusion as to whether κ is higher or lower than that of diamond, and/or the measurements were performed on nonpristine graphene. Future measurements on pristine graphene with significantly reduced uncertainty are needed to test our prediction. Another consequence of our results is that the predicted graphene thermal conductivity is lower than the experimentally reported κ of graphite [60,61] [Fig. 4(b)]. Theoretical study of graphite considering both four-phonon scattering and phonon renormalization is not yet seen in the literature. Future studies could be focusing on the layer-dependent transport behavior of multilayer graphene and graphite. We expect such comparison may motivate further experimental efforts to fully resolve the intriguing finding here. A tentative explanation might be that in bulk-phase graphite, the four-phonon scattering of the ZA mode is suppressed by interlayer interactions. Also, the previous 4ph modeling [27] suggests that in graphite, four-ZA scattering phase space is reduced by 16 times compared to graphene and one may expect 4ph scattering to be weak.

In summary, we conduct a first-principles study on the thermal conductivity of monolayer graphene. Our calculations include four-phonon scattering, phonon renormalization effect, and the exact solution to BTE, all of which are state-of-the-art computational formalism. Our methods can reveal both phonon properties, their detailed scatterings, and eventually the thermal conductivity of graphene over a wide range of temperature. Our results in this work provide a strong computational evidence of κ convergence to date. We expect our study to inspire further experimental efforts on graphene and theoretical understanding of general low-dimensional systems.

We are grateful for the insightful discussions with Prof. Li Shi at the University of Texas at Austin. X.R. and Z.H. were supported by the U.S. National Science Foundation (Grants No. 2015946 and No. 2321301). Simulations were performed at the Rosen Center for Advanced Computing (RCAC) of Purdue University.

[1] K. S. Novoselov, A. K. Geim, S. V. Morozov, D. Jiang, Y. Zhang, S. V. Dubonos, I. V. Grigorieva, and A. A. Firsov, Electric field effect in atomically thin carbon films, Science **306**, 666 (2004).

[2] Y. Zhang, Y.-W. Tan, H. L. Stormer, and P. Kim, Experimental observation of the quantum Hall effect and Berry's phase in graphene, Nature (London) **438**, 201 (2005).

[3] A. K. Geim and K. S. Novoselov, The rise of graphene, Nat. Mater. **6**, 183 (2007).

[4] R. R. Nair, P. Blake, A. N. Grigorenko, K. S. Novoselov, T. J. Booth, T. Stauber, N. M. R. Peres, and A. K. Geim, Fine structure constant defines visual transparency of graphene, Science **320**, 1308 (2008).

[5] S. Ghosh, I. Calizo, D. Teweldebrhan, E. P. Pokatilov, D. L. Nika, A. A. Balandin, W. Bao, F. Miao, and C. N. Lau, Extremely high thermal conductivity of graphene: Prospects for thermal management applications in nanoelectronic circuits, Appl. Phys. Lett. **92**, 151911 (2008).

[6] F. Bonaccorso, Z. Sun, T. Hasan, and A. Ferrari, Graphene photonics and optoelectronics, Nat. Photon. **4**, 611 (2010).

[7] A. A. Balandin, S. Ghosh, W. Bao, I. Calizo, D. Teweldebrhan, F. Miao, and C. N. Lau, Superior thermal conductivity of single-layer graphene, Nano Lett. **8**, 902 (2008).

[8] L. Lindsay, D. A. Broido, and N. Mingo, Flexural phonons and thermal transport in graphene, Phys. Rev. B **82**, 115427 (2010).

[9] L. Lindsay, W. Li, J. Carrete, N. Mingo, D. A. Broido, and T. L. Reinecke, Phonon thermal transport in strained and unstrained graphene from first principles, Phys. Rev. B **89**, 155426 (2014).

[10] G. Fugallo, A. Cepellotti, L. Paulatto, M. Lazzeri, N. Marzari, and F. Mauri, Thermal conductivity of graphene and graphite: Collective excitations and mean free paths, Nano Lett. **14**, 6109 (2014).

[11] D. Singh, J. Y. Murthy, and T. S. Fisher, Mechanism of thermal conductivity reduction in few-layer graphene, J. Appl. Phys. **110**, 044317 (2011).

[12] X. Xu, L. F. C. Pereira, Y. Wang, J. Wu, K. Zhang, X. Zhao, S. Bae, C. T. Bui, R. Xie, J. T. L. Thong, B. H. Hong, K. P. Loh, D. Donadio, B. Li, and B. Özyilmaz, Length-dependent thermal conductivity in suspended single-layer graphene, Nat. Commun. **5**, 3689 (2014).

[13] S. Chen, A. L. Moore, W. Cai, J. W. Suk, J. An, C. Mishra, C. Amos, C. W. Magnuson, J. Kang, L. Shi, and R. S. Ruoff, Raman measurements of thermal transport in suspended monolayer graphene of variable sizes in vacuum and gaseous environments, ACS Nano **5**, 321 (2011).

[14] C. Faugeras, B. Faugeras, M. Orlita, M. Potemski, R. R. Nair, and A. K. Geim, Thermal conductivity of graphene in corbino membrane geometry, ACS Nano **4**, 1889 (2010).

[15] J.-U. Lee, D. Yoon, H. Kim, S. W. Lee, and H. Cheong, Thermal conductivity of suspended pristine graphene measured by Raman spectroscopy, Phys. Rev. B **83**, 081419(R) (2011).

[16] A. K. Vallabhaneni, D. Singh, H. Bao, J. Murthy, and X. Ruan, Reliability of Raman measurements of thermal conductivity of single-layer graphene due to selective electron-phonon coupling: A first-principles study, Phys. Rev. B **93**, 125432 (2016).

[17] S. Sullivan, A. Vallabhaneni, I. Kholmanov, X. Ruan, J. Murthy, and L. Shi, Optical generation and detection of local nonequilibrium phonons in suspended graphene, Nano Lett. **17**, 2049 (2017).

[18] E. Mariani and F. von Oppen, Flexural Phonons in Free-Standing Graphene, Phys. Rev. Lett. **100**, 076801 (2008).

[19] E. Fermi, P. Pasta, S. Ulam, and M. Tsingou, Studies of the nonlinear problems, Tech. Rep. No. LA-1940 (Los Alamos National Laboratory, Los Alamos, New Mexico, 1955).

[20] *Thermal Transport in Low Dimensions, From Statistical Physics to Nanoscale Heat Transfer*, Lecture Notes in Physics Vol. 921, edited by S. Lepri (Springer International, Switzerland, 2016).

[21] G. Basile, C. Bernardin, and S. Olla, Momentum Conserving Model with Anomalous Thermal Conductivity in Low Dimensional Systems, Phys. Rev. Lett. **96**, 204303 (2006).

[22] L. Wang, B. Hu, and B. Li, Logarithmic divergent thermal conductivity in two-dimensional nonlinear lattices, Phys. Rev. E **86**, 040101(R) (2012).

[23] T. Feng and X. Ruan, Quantum mechanical prediction of four-phonon scattering rates and reduced thermal conductivity of solids, Phys. Rev. B **93**, 045202 (2016).

[24] T. Feng, L. Lindsay, and X. Ruan, Four-phonon scattering significantly reduces intrinsic thermal conductivity of solids, Phys. Rev. B **96**, 161201(R) (2017).

[25] Y. Xia, V. I. Hegde, K. Pal, X. Hua, D. Gaines, S. Patel, J. He, M. Aykol, and C. Wolverton, High-Throughput Study of Lattice Thermal Conductivity in Binary Rocksalt and Zinc Blende Compounds Including Higher-Order Anharmonicity, Phys. Rev. X **10**, 041029 (2020).

[26] N. K. Ravichandran and D. Broido, Phonon-Phonon Interactions in Strongly Bonded Solids: Selection Rules and Higher-Order Processes, Phys. Rev. X **10**, 021063 (2020).

[27] T. Feng and X. Ruan, Four-phonon scattering reduces intrinsic thermal conductivity of graphene and the contributions from flexural phonons, Phys. Rev. B **97**, 045202 (2018).

[28] X. Gu, Z. Fan, H. Bao, and C. Y. Zhao, Revisiting phonon-phonon scattering in single-layer graphene, Phys. Rev. B **100**, 064306 (2019).

[29] B. Qiu and X. Ruan, Reduction of spectral phonon relaxation times from suspended to supported graphene, Appl. Phys. Lett. **100**, 193101 (2012).

[30] L. F. C. Pereira and D. Donadio, Divergence of the thermal conductivity in uniaxially strained graphene, Phys. Rev. B **87**, 125424 (2013).

[31] Z. Fan, L. F. C. Pereira, P. Hirvonen, M. M. Ervasti, K. R. Elder, D. Donadio, T. Ala-Nissila, and A. Harju, Thermal conductivity decomposition in two-dimensional materials: Application to graphene, Phys. Rev. B **95**, 144309 (2017).

[32] U. Ray and D. T. Limmer, Heat current fluctuations and anomalous transport in low-dimensional carbon lattices, Phys. Rev. B **100**, 241409(R) (2019).

[33] G. Barbarino, C. Melis, and L. Colombo, Intrinsic thermal conductivity in monolayer graphene is ultimately upper limited: A direct estimation by atomistic simulations, Phys. Rev. B **91**, 035416 (2015).

[34] H. P. C. Miranda, henriquemiranda.github.io/phononwebsite/index.html, a tool to visualize phonon vibrational modes.

[35] O. Hellman, I. A. Abrikosov, and S. I. Simak, Lattice dynamics of anharmonic solids from first principles, Phys. Rev. B **84**, 180301(R) (2011).

[36] O. Hellman, P. Steneteg, I. A. Abrikosov, and S. I. Simak, Temperature dependent effective potential method for accurate free energy calculations of solids, Phys. Rev. B **87**, 104111 (2013).

[37] O. Hellman and I. A. Abrikosov, Temperature-dependent effective third-order interatomic force constants from first principles, Phys. Rev. B **88**, 144301 (2013).

[38] D. S. Kim, O. Hellman, J. Herriman, H. L. Smith, J. Y. Y. Lin, N. Shulumba, J. L. Niedziela, C. W. Li, D. L. Abernathy, and B. Fultz, Nuclear quantum effect with pure anharmonicity and the anomalous thermal expansion of silicon, Proc. Natl. Acad. Sci. USA **115**, 1992 (2018).

[39] N. K. Ravichandran and D. Broido, Unified first-principles theory of thermal properties of insulators, Phys. Rev. B **98**, 085205 (2018).

[40] Y. Xia and M. K. Y. Chan, Anharmonic stabilization and lattice heat transport in rocksalt β-GeTe, Appl. Phys. Lett. **113**, 193902 (2018).

[41] Z. Han, X. Yang, S. E. Sullivan, T. Feng, L. Shi, W. Li, and X. Ruan, Raman Linewidth Contributions from Four-Phonon and Electron-Phonon Interactions in Graphene, Phys. Rev. Lett. **128**, 045901 (2022).

[42] M. Omini and A. Sparavigna, An iterative approach to the phonon Boltzmann equation in the theory of thermal conductivity, Phys. B: Condens. Matter **212**, 101 (1995).

[43] G. Kresse and J. Hafner, *Ab initio* molecular dynamics for liquid metals, Phys. Rev. B **47**, 558 (1993).

[44] J. M. Ziman, *Electrons and Phonons: The Theory of Transport Phenomena in Solids*, International Series of Monographs on Physics (Clarendon Press, Oxford, 1960).

[45] Z. Han, X. Yang, W. Li, T. Feng, and X. Ruan, Four-Phonon: An extension module to ShengBTE for computing four-phonon scattering rates and thermal conductivity, Comput. Phys. Commun. **270**, 108179 (2022).

[46] W. Li, J. Carrete, N. A. Katcho, and N. Mingo, ShengBTE: A solver of the Boltzmann transport equation for phonons, Comput. Phys. Commun. **185**, 1747 (2014).

[47] Incorporating four-phonon scattering to the iterative solver is nontrivial since the scattering matrix and phonon information consume a great amount of storage. For future usage and community adoption, we use OpenMP parallelism to store the scattering matrix in memory. The memory consumption scales

with the mesh size N to the fifth power. The largest mesh size case can be done on a flat node equipped with 1 TB memory.

[48] X. Yang, T. Feng, J. S. Kang, Y. Hu, J. Li, and X. Ruan, Observation of strong higher-order lattice anharmonicity in Raman and infrared spectra, Phys. Rev. B **101**, 161202(R) (2020).

[49] J. H. Seol, I. Jo, A. L. Moore, L. Lindsay, Z. H. Aitken, M. T. Pettes, X. Li, Z. Yao, R. Huang, D. Broido, N. Mingo, R. S. Ruoff, and L. Shi, Two-dimensional phonon transport in supported graphene, Science **328**, 213 (2010).

[50] S. Lee, D. Broido, K. Esfarjani, and G. Chen, Hydrodynamic phonon transport in suspended graphene, Nat. Commun. **6**, 6290 (2015).

[51] A. Cepellotti, G. Fugallo, L. Paulatto, M. Lazzeri, F. Mauri, and N. Marzari, Phonon hydrodynamics in two-dimensional materials, Nat. Commun. **6**, 6400 (2015).

[52] See Supplemental Material at http://link.aps.org/supplemental/10.1103/PhysRevB.108.L121412 for computational details, BTE solutions, detailed formalism, along with phonon mean free path, and comparison to prior studies (see, also, Refs. [63–65] therein).

[53] N. Mingo and D. A. Broido, Length dependence of carbon nanotube thermal conductivity and the "problem of long waves", Nano Lett. **5**, 1221 (2005).

[54] G. Barbalinardo, Z. Chen, H. Dong, Z. Fan, and D. Donadio, Ultrahigh Convergent Thermal Conductivity of Carbon Nanotubes from Comprehensive Atomistic Modeling, Phys. Rev. Lett. **127**, 025902 (2021).

[55] D. Bruns, A. Nojeh, A. S. Phani, and J. Rottler, Comment on "Ultrahigh Convergent Thermal Conductivity of Carbon Nanotubes from Comprehensive Atomistic Modeling," Phys. Rev. Lett. **128**, 259601 (2022).

[56] G. Barbalinardo, Z. Chen, H. Dong, Z. Fan, and D. Donadio, Barbalinardo *et al.* Reply:, Phys. Rev. Lett. **128**, 259602 (2022).

[57] L. Wei, P. K. Kuo, R. L. Thomas, T. R. Anthony, and W. F. Banholzer, Thermal Conductivity of Isotopically Modified Single Crystal Diamond, Phys. Rev. Lett. **70**, 3764 (1993).

[58] J. R. Olson, R. O. Pohl, J. W. Vandersande, A. Zoltan, T. R. Anthony, and W. F. Banholzer, Thermal conductivity of diamond between 170 and 1200 K and the isotope effect, Phys. Rev. B **47**, 14850 (1993).

[59] D. G. Onn, A. Witek, Y. Z. Qiu, T. R. Anthony, and W. F. Banholzer, Some Aspects of the Thermal Conductivity of Isotopically Enriched Diamond Single Crystals, Phys. Rev. Lett. **68**, 2806 (1992).

[60] R. Taylor, The thermal conductivity of pyrolytic graphite, Philos. Mag. **13**, 157 (1966).

[61] C. Y. Ho, R. W. Powell, and P. E. Liley, Thermal conductivity of the elements: A comprehensive review, J. Phys. Chem. Ref. Data, Suppl. **3**, 1 (1974).

[62] R. Berman, P. R. W. Hudson, and M. Martinez, Nitrogen in diamond: Evidence from thermal conductivity, J. Phys. C **8**, L430 (1975).

[63] J. P. Perdew, K. Burke, and M. Ernzerhof, Generalized Gradient Approximation Made Simple, Phys. Rev. Lett. **77**, 3865 (1996).

[64] A. A. Maradudin and A. E. Fein, Scattering of neutrons by an anharmonic crystal, Phys. Rev. **128**, 2589 (1962).

[65] F. Tian, B. Song, X. Chen, N. K. Ravichandran, Y. Lv, K. Chen, S. Sullivan, J. Kim, Y. Zhou, T.-H. Liu, M. Goni, Z. Ding, J. Sun, G. A. G. U. Gamage, H. Sun, H. Ziyaee, S. Huyan, L. Deng, J. Zhou, A. J. Schmidt *et al.*, Unusual high thermal conductivity in boron arsenide bulk crystals, Science **361**, 582 (2018).

Supplemental Material for "Thermal conductivity in pristine graphene: Convergent and lower than diamond"

Zherui Han[1] and Xiulin Ruan[1,*]

[1] *School of Mechanical Engineering and the Birck Nanotechnology Center, Purdue University, West Lafayette, Indiana 47907-2088, USA*

(Dated: September 16, 2023)

CONTENTS

COMPUTATIONAL DETAILS

We consider naturally occurring, monolayer graphene in our simulation with a vacuum space of 14 Å between periodic graphene layers. We employ VASP package [1] and use Perdew-Burke-Ernzerhof (PBE) parameterization of the generalized gradient approximation (GGA) for exchange and correlation functionals [2]. The plane wave cutoff is 600 eV. For the ground state, we construct $8\times8\times1$ supercells and use $3\times3\times1$ k-mesh to calculate interatomic force constants (IFCs) and consider the tenth and second nearest neighboring atoms for third-order IFCs and fourth-order IFCs, respectively.

To consider the phonon renormalization at finite temperatures in graphene, we choose TDEP developed by Hellman et al., since it is compatible with ab initio calculations and can simulate thermal displacements of atoms using Bose–Einstein distribution [3–5]. The key of this method is to obtain effective IFCs at finite-temperatures that can fit into forces-displacements data. We employ a $10\times10\times1$ supercell of graphene and iterate the calculations using 100 thermally perturbed snapshots. At each temperature, the last iteration is done using 400 snapshots to ensure convergence and three iterations are sufficient in our calculations. Anharmonic temperature-dependent IFCs have the same number of many-body interactions as the ground-state IFCs. These IFCs are the same as what we have calculated in our prior work [6].

ITERATIVE SCHEME TO PHONON BTE

The linearized phonon Boltzmann transport equation with three-phonon scattering has been extensively studied in the literature [7], and the formalism on four-phonon scattering has also been well documented in several preceding papers [8–12]. In this section we cover our implementation of iterative scheme to phonon BTE, which has been discussed in our previous work [12]. At steady state, the rate of change of phonon distribution function due to diffusion and scattering should be balanced out for a certain phonon mode λ:

$$\frac{\partial n_\lambda}{\partial t}=\left.\frac{\partial n_\lambda}{\partial t}\right|_{\text{diff}}+\left.\frac{\partial n_\lambda}{\partial t}\right|_{\text{scatt}}\equiv0. \tag{S.1}$$

Using the relaxation time approximation (RTA), the scattering term is expressed as: $\left.\frac{\partial n_\lambda}{\partial t}\right|_{\text{scatt}}=\frac{n_\lambda-n_\lambda^0}{\tau_\lambda}$, where n_λ^0 and τ_λ are the equilibrium Bose-Einstein distribution and the relaxation time for phonon mode λ. The diffusion term is $\left.\frac{\partial n_\lambda}{\partial t}\right|_{\text{diff}}=-\frac{\partial n_\lambda}{\partial T}\nabla T\cdot\mathbf{v}_\lambda$ with $\mathbf{v}_\lambda$ being the group velocity. It is convenient to write the equation in terms of the deviation from of $n_\lambda=n_\lambda^0-\mathbf{F}_\lambda\cdot\frac{\partial n_\lambda}{\partial T}\nabla T-...$, and only keep the linear terms with $\mathbf{F}_\lambda$ in the scattering term.

Then, for a certain mode λ, the linearized BTE [13] is expressed as:

$$\mathbf{F}_\lambda=\tau_\lambda^0(\mathbf{v}_\lambda+\mathbf{\Delta}_\lambda), \tag{S.2}$$

where τ_λ^0 is the relaxation time for mode λ under RTA. $\mathbf{\Delta}_\lambda$ works for iterative scheme and is a quantity showing the phonon population deviation from the RTA scheme. With the inclusion of four-phonon scattering, $\mathbf{\Delta}_\lambda$ and τ_λ^0 (0 represents zeroth-order in iterations) are computed as:

$$\begin{aligned}\mathbf{\Delta}_\lambda=&\frac{1}{N_q}\sum_{\lambda'\lambda''}^{(+)}\Gamma^{(+)}_{\lambda\lambda'\lambda''}(\xi_{\lambda\lambda''}\mathbf{F}_{\lambda''}-\xi_{\lambda\lambda'}\mathbf{F}_{\lambda'})+\frac{1}{N_q}\sum_{\lambda'\lambda''}^{(-)}\frac{1}{2}\Gamma^{(-)}_{\lambda\lambda'\lambda''}(\xi_{\lambda\lambda''}\mathbf{F}_{\lambda''}+\xi_{\lambda\lambda'}\mathbf{F}_{\lambda'})\\&\left.\begin{aligned}&+\tfrac{1}{N_q}\sum_{\lambda'\lambda''\lambda'''}^{(++)}\frac{1}{2}\Gamma^{(++)}_{\lambda\lambda'\lambda''\lambda'''}(\xi_{\lambda\lambda'''}\mathbf{F}_{\lambda'''}-\xi_{\lambda\lambda'}\mathbf{F}_{\lambda'}-\xi_{\lambda\lambda''}\mathbf{F}_{\lambda''})\\&+\tfrac{1}{N_q}\sum_{\lambda'\lambda''\lambda'''}^{(+-)}\frac{1}{2}\Gamma^{(+-)}_{\lambda\lambda'\lambda''\lambda'''}(\xi_{\lambda\lambda'''}\mathbf{F}_{\lambda'''}-\xi_{\lambda\lambda'}\mathbf{F}_{\lambda'}+\xi_{\lambda\lambda''}\mathbf{F}_{\lambda''})\\&+\tfrac{1}{N_q}\sum_{\lambda'\lambda''\lambda'''}^{(--)}\frac{1}{6}\Gamma^{(--)}_{\lambda\lambda'\lambda''\lambda'''}(\xi_{\lambda\lambda'''}\mathbf{F}_{\lambda'''}+\xi_{\lambda\lambda'}\mathbf{F}_{\lambda'}+\xi_{\lambda\lambda''}\mathbf{F}_{\lambda''})\end{aligned}\right\}\text{four-phonon terms}\\&+\frac{1}{N_q}\sum_{\lambda'}^{(\text{iso})}\Gamma^{(\text{iso})}_{\lambda\lambda'}\xi_{\lambda\lambda'}\mathbf{F}_{\lambda'},\end{aligned} \tag{S.3}$$

$$\frac{1}{\tau_\lambda^0} = \frac{1}{N_q}\left(\sum_{\lambda'\lambda''}^{(+)}\Gamma^{(+)}_{\lambda\lambda'\lambda''} + \sum_{\lambda'\lambda''}^{(-)}\frac{1}{2}\Gamma^{(-)}_{\lambda\lambda'\lambda''}\right) + \frac{1}{N_q}\sum_{\lambda'}^{(\mathrm{iso})}\Gamma^{(\mathrm{iso})}_{\lambda\lambda'} + \underbrace{\frac{1}{N_q}\left(\sum_{\lambda'\lambda''\lambda'''}^{(++)}\frac{1}{2}\Gamma^{(++)}_{\lambda\lambda'\lambda''\lambda'''} + \sum_{\lambda'\lambda''\lambda'''}^{(+-)}\frac{1}{2}\Gamma^{(+-)}_{\lambda\lambda'\lambda''\lambda'''} + \sum_{\lambda'\lambda''\lambda'''}^{(--)}\frac{1}{6}\Gamma^{(--)}_{\lambda\lambda'\lambda''\lambda'''}\right)}_{\text{four-phonon scattering terms}}, \tag{S.4}$$

where N_q is the total grid of $\mathbf{q}$ points. $\xi_{\lambda\lambda'} = \omega_{\lambda'}/\omega_{\lambda''}$. The superscripts $(\pm)$ or $(\pm\pm)$ represent the three-phonon (3ph) and four-phonon (4ph) processes, namely $\mathbf{q}'' = \mathbf{q} \pm \mathbf{q}' + \mathbf{Q}$ and $\mathbf{q}''' = \mathbf{q} \pm \mathbf{q}' \pm \mathbf{q}'' + \mathbf{Q}$, respectively. $\mathbf{Q}$ is a reciprocal lattice vector with $\mathbf{Q} = 0$ implying normal process. Inspecting the expression of Eq. S.3 along with Eq. S.2, we find that the solution of $\mathbf{F}_\lambda$ requires the self-consistent solutions of the same quantity of all other phonon modes since they appear in the right-hand-side of Eq. S.2. Our iterative scheme then takes $\mathbf{F}_\lambda^0 = \tau_\lambda^0\mathbf{v}_\lambda$ as initial guess and solves Eq. S.2 iteratively.

$\Gamma^{(\mathrm{iso})}$ is the isotope scattering rates. Other Γ with superscripts denote the scattering rates for 3ph and 4ph processes, and the scattering probability matrices are [8, 14]:

$$\begin{aligned}
\Gamma^{(+)}_{\lambda\lambda'\lambda''} &= \frac{\hbar\pi}{4}\frac{n^0_{\lambda'} - n^0_{\lambda''}}{\omega_\lambda\omega_{\lambda'}\omega_{\lambda''}}|V^{(+)}_{\lambda\lambda'\lambda''}|^2\delta(\omega_\lambda + \omega_{\lambda'} - \omega_{\lambda''}) \\
\Gamma^{(-)}_{\lambda\lambda'\lambda''} &= \frac{\hbar\pi}{4}\frac{n^0_{\lambda'} + n^0_{\lambda''} + 1}{\omega_\lambda\omega_{\lambda'}\omega_{\lambda''}}|V^{(-)}_{\lambda\lambda'\lambda''}|^2\delta(\omega_\lambda - \omega_{\lambda'} - \omega_{\lambda''}),
\end{aligned} \tag{S.5}$$

$$\begin{aligned}
\Gamma^{(++)}_{\lambda\lambda'\lambda''\lambda'''} &= \frac{\hbar^2\pi}{8N_q}\frac{(1+n^0_{\lambda'})(1+n^0_{\lambda''})n^0_{\lambda'''}}{n^0_\lambda}|V^{(++)}_{\lambda\lambda'\lambda''\lambda'''}|^2\frac{\delta(\omega_\lambda + \omega_{\lambda'} + \omega_{\lambda''} - \omega_{\lambda'''})}{\omega_\lambda\omega_{\lambda'}\omega_{\lambda''}\omega_{\lambda'''}} \\
\Gamma^{(+-)}_{\lambda\lambda'\lambda''\lambda'''} &= \frac{\hbar^2\pi}{8N_q}\frac{(1+n^0_{\lambda'})n^0_{\lambda''}n^0_{\lambda'''}}{n^0_\lambda}|V^{(+-)}_{\lambda\lambda'\lambda''\lambda'''}|^2\frac{\delta(\omega_\lambda + \omega_{\lambda'} - \omega_{\lambda''} - \omega_{\lambda'''})}{\omega_\lambda\omega_{\lambda'}\omega_{\lambda''}\omega_{\lambda'''}} \\
\Gamma^{(--)}_{\lambda\lambda'\lambda''\lambda'''} &= \frac{\hbar^2\pi}{8N_q}\frac{n^0_{\lambda'}n^0_{\lambda''}n^0_{\lambda'''}}{n^0_\lambda}|V^{(--)}_{\lambda\lambda'\lambda''\lambda'''}|^2\frac{\delta(\omega_\lambda - \omega_{\lambda'} - \omega_{\lambda''} - \omega_{\lambda'''})}{\omega_\lambda\omega_{\lambda'}\omega_{\lambda''}\omega_{\lambda'''}},
\end{aligned} \tag{S.6}$$

where Eq. (S.5) is for three-phonon processes and Eq. (S.6) for the four-phonon processes, with n^0_λ being the phonon Bose-Einstein distribution at equilibrium, ω_λ being the phonon frequency for a certain mode λ. Conservation of energy is enforced by the Dirac delta function δ and is approximated by an adaptive Gaussian broadening [12]. In Eqs. (S.5) and (S.6), the matrix elements V are given by the Fourier transformation of force constants, or transition probability matrices:

$$V^{(\pm)}_{\lambda\lambda'\lambda''} = \sum_{ijk}\sum_{\alpha\beta\gamma}\Phi^{\alpha\beta\gamma}_{ijk}\frac{e^\lambda_\alpha(i)e^{\pm\lambda'}_\beta(j)e^{-\lambda''}_\gamma(k)}{\sqrt{M_iM_jM_k}}e^{\pm i\mathbf{q}'\cdot\mathbf{r}_j}e^{-i\mathbf{q}''\cdot\mathbf{r}_k}, \tag{S.7}$$

$$V^{(\pm\pm)}_{\lambda\lambda'\lambda''\lambda'''} = \sum_{ijkl}\sum_{\alpha\beta\gamma\theta}\Phi^{\alpha\beta\gamma\theta}_{ijkl}\frac{e^\lambda_\alpha(i)e^{\pm\lambda'}_\beta(j)e^{\pm\lambda''}_\gamma(k)e^{-\lambda'''}_\theta(l)}{\sqrt{M_iM_jM_kM_l}}e^{\pm i\mathbf{q}'\cdot\mathbf{r}_j}e^{\pm i\mathbf{q}''\cdot\mathbf{r}_k}e^{-i\mathbf{q}'''\cdot\mathbf{r}_l}, \tag{S.8}$$

where i, j, k, l denote the atomic indices and $\alpha, \beta, \gamma, \theta$ denote the Cartesian dimensions x, y or z. $\Phi^{\alpha\beta\gamma}_{ijk}$ and $\Phi^{\alpha\beta\gamma\theta}_{ijkl}$ are the third-order and fourth-order force constants, respectively. $e^\lambda_\alpha(i)$ is the eigenvector component for a mode. $\mathbf{r}_j$ is the position vector of the unit cell where jth atom lies, and M_j is its mass.

Finally, the lattice thermal conductivity tensor is computed as [7, 15]:

$$\kappa^{\alpha\beta} = \frac{1}{k_\mathrm{B}T^2\Omega N_q}\sum_\lambda n^0\left(n^0+1\right)\left(\hbar\omega_\lambda\right)^2 v^\alpha_\lambda F^\beta_\lambda, \tag{S.9}$$

where Ω is the volume of the unit cell and in the case of monolayer graphene, Ω should be 2D area times the separation of carbon sheets in graphite ($d = 3.35$ Å) [16]. The component in this expression is the self-consistent solution $\mathbf{F}_\lambda$. The stopping criterion is that the norm of κ tensor differs from the last iteration within 10^{-5}.

To iteratively solve BTE with 4ph scattering, one needs to store the scattering matrix and phonon information which consume a great amount of memory space. We use a shared-memory parallel computing strategy under OpenMP architecture. The empirical scaling of memory M with respect to mesh size N is plotted in Fig. S1. If the allowable memory is 1 TB which is accessible in some supercomputer clusters equipped with flat nodes, then the maximum mesh size is $54 \times 54 \times 1$.

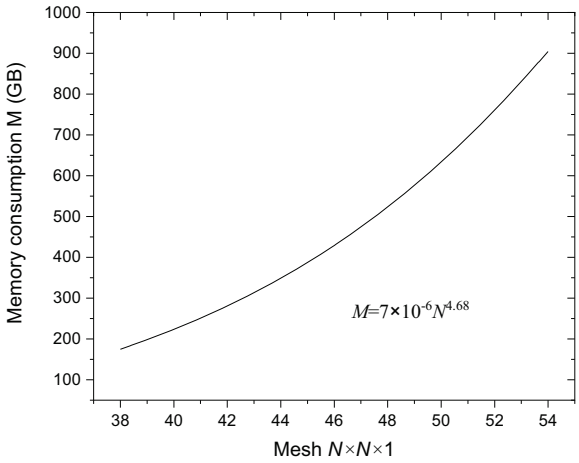

FIG. S1. Scaling relation of memory consumption M and mesh size N.

COMPARISON OF THE RELAXATION TIME APPROXIMATION AND ITERATIVE SOLUTION

The exact solution of phonon BTE through the iterative scheme naturally capture the collective phonon excitations. Compared to RTA where phonons behave independently after the scattering events, in the exact BTE the phonon populations are coupled with each other. For graphene, a large portion of scattering events is normal processes that contribute indirectly to thermal resistance. Thus, phonons expect to have strong deviations from RTA-rendered populations and the iterative result of κ is different from RTA solution.

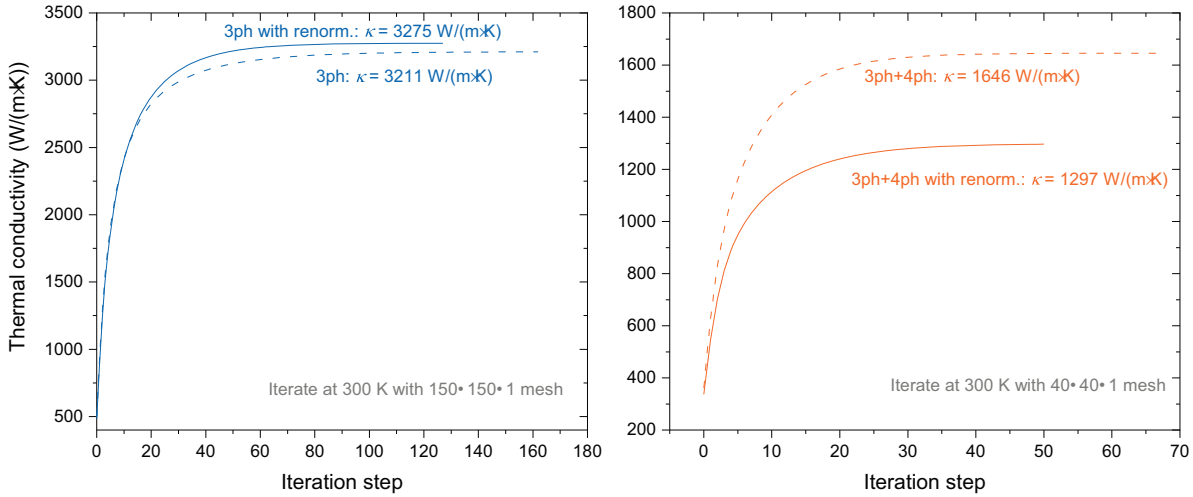

FIG. S2. Comparison of RTA (iteration step equals zero) and iterative results for $\kappa_{3\mathrm{ph}}$ (left) and $\kappa_{3\mathrm{ph+4ph}}$ (right) of naturally occurring graphene. In this figure, *renorm.* stands for renormalization. The $x-$axis is the number of iteration step in the self-consistent solver.

Figure S2 shows that for both 3ph and 4ph scattering, thermal conductivity from iterative result has about six folds increase compared to RTA. The collective phonon excitation in graphene cannot be neglected. Another observation

is that the phonon renormalization effect impacts $\kappa_{3ph+4ph}$ more than κ_{3ph}. The renormalization increases κ_{3ph} while decreases $\kappa_{3ph+4ph}$. This is primarily due to the impact of renormalization on ZA phonons scattering rates at room temperature. After renormalization, 4ph scattering rates of ZA modes are higher while 3ph scattering rates are not much affected.

COMPARISON OF OUR THREE-PHONON RESULTS AND THE LITERATURE

Since the previous first-principles results did not include higher-order anharmonicity or the phonon renormalization, a fair comparison should be between their results and our DFT results at 3ph level without phonon renormalization. The sample size is chosen to be finite (L = 10 μm) to ensure convergence. The temperature-dependent thermal conductivity from prior DFT studies [16, 17] is presented with our results in Fig. S3. Our results somewhat lie between these two reports.

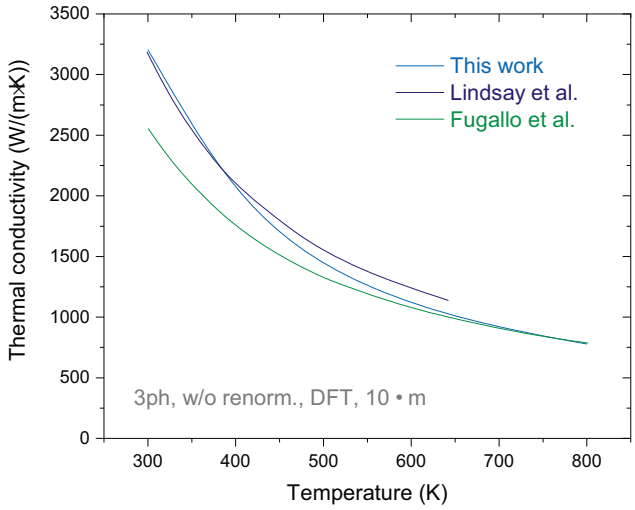

FIG. S3. Comparison of our 3ph scattering results with the previous DFT simulations at 3ph level. In this work, the energy broadening factor is unity.

PHONON MEAN FREE PATH ACCUMULATION IN GRAPHENE

The thermal conductivity accumulation as a function of mean free path is presented in Fig. S4. This quantity has implications in length-dependent thermal conductivity that may be measured in experiments. It is also useful to estimate the length scale of thermal conductivity to reach the diffusive limit [17]. Our simulation results indicate that this diffusive limit may be reached around 10 μm. For 3ph theory, thermal conductivity does not converge with mesh size. In the plot Fig. S4, with greater mesh size N phonons with larger mean free path keep contributing to thermal conductivity.

We further calculate the length-dependent thermal conductivity of graphene with four-phonon scattering considered. The boundary scattering term is described in the main text. Distinct with prior theoretical reports [16, 18], our results show a converged length dependence. At L = 10 μm, thermal conductivity is 1247 W/(m·K), only 4% different compared to the intrinsic value.

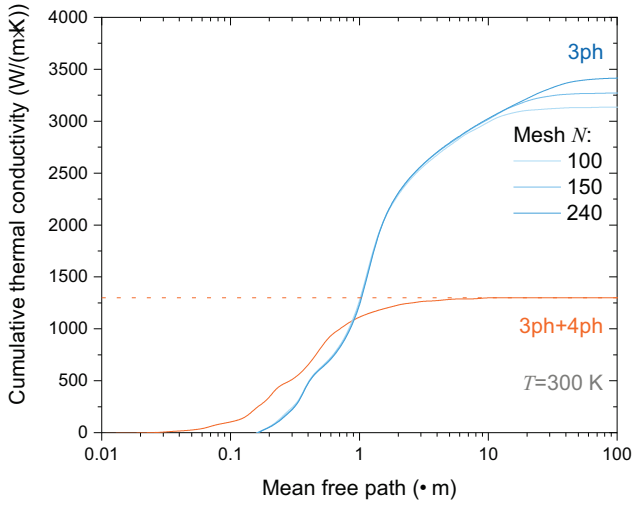

FIG. S4. Room temperature thermal conductivity as a function of phonon mean free path at 3ph and 3ph+4ph level. The $x-$axis is presented in logrithm scale. The dotted line shows the converged thermal conductivity without boundary. Curves with different blue colors represent the results from different mesh size. Clearly κ converges with system (mesh) size and mean free path under 3ph+4ph picture, but does not converge under 3ph picture.

* ruan@purdue.edu

[1] G. Kresse and J. Hafner, Ab initio molecular dynamics for liquid metals, Phys. Rev. B **47**, 558 (1993).

[2] J. P. Perdew, K. Burke, and M. Ernzerhof, Generalized Gradient Approximation Made Simple, Phys. Rev. Lett. **77**, 3865 (1996).

[3] O. Hellman, P. Steneteg, I. A. Abrikosov, and S. I. Simak, Temperature dependent effective potential method for accurate free energy calculations of solids, Physical Review B **87**, 104111 (2013), 1303.1145.

[4] O. Hellman and I. A. Abrikosov, Temperature-dependent effective third-order interatomic force constants from first principles, Physical Review B **88**, 144301 (2013).

[5] D. S. Kim, O. Hellman, J. Herriman, H. L. Smith, J. Y. Y. Lin, N. Shulumba, J. L. Niedziela, C. W. Li, D. L. Abernathy, and B. Fultz, Nuclear quantum effect with pure anharmonicity and the anomalous thermal expansion of silicon, Proceedings of the National Academy of Sciences **115**, 1992 (2018), 1610.08737.

[6] Z. Han, X. Yang, S. E. Sullivan, T. Feng, L. Shi, W. Li, and X. Ruan, Raman Linewidth Contributions from Four-Phonon and Electron-Phonon Interactions in Graphene, Physical Review Letters **128**, 045901 (2022).

[7] W. Li, J. Carrete, N. A. Katcho, and N. Mingo, ShengBTE: A solver of the Boltzmann transport equation for phonons, Comput. Phys. Commun. **185**, 1747 (2014).

[8] T. Feng and X. Ruan, Quantum mechanical prediction of four-phonon scattering rates and reduced thermal conductivity of solids, Physical Review B **93**, 045202 (2016).

[9] T. Feng, L. Lindsay, and X. Ruan, Four-phonon scattering significantly reduces intrinsic thermal conductivity of solids, Physical Review B **96**, 161201 (2017).

[10] T. Feng and X. Ruan, Four-phonon scattering reduces intrinsic thermal conductivity of graphene and the contributions from flexural phonons, Physical Review B **97**, 045202 (2018).

[11] F. Tian, B. Song, X. Chen, N. K. Ravichandran, Y. Lv, K. Chen, S. Sullivan, J. Kim, Y. Zhou, T.-H. Liu, M. Goni, Z. Ding, J. Sun, G. A. G. U. Gamage, H. Sun, H. Ziyaee, S. Huyan, L. Deng, J. Zhou, A. J. Schmidt, S. Chen, C.-W. Chu, P. Y. Huang, D. Broido, L. Shi, G. Chen, and Z. Ren, Unusual high thermal conductivity in boron arsenide bulk crystals, Science **361**, 582 (2018).

[12] Z. Han, X. Yang, W. Li, T. Feng, and X. Ruan, FourPhonon: An extension module to ShengBTE for computing four-phonon scattering rates and thermal conductivity, Comput. Phys. Commun. **270**, 108179 (2022).

[13] M. Omini and A. Sparavigna, An iterative approach to the phonon Boltzmann equation in the theory of thermal conductivity, Physica B: Condensed Matter **212**, 101 (1995).

[14] A. A. Maradudin and A. E. Fein, Scattering of neutrons by an anharmonic crystal, Physical Review **128**, 2589 (1962).

[15] J. M. Ziman, *Electrons and phonons: the theory of transport phenomena in solids*, International series of monographs on physics (Oxford, England) (Clarendon Press, Oxford, 1960).

[16] L. Lindsay, W. Li, J. Carrete, N. Mingo, D. A. Broido, and T. L. Reinecke, Phonon thermal transport in strained and unstrained graphene from first principles, Physical Review B **89**, 155426 (2014).

[17] G. Fugallo, A. Cepellotti, L. Paulatto, M. Lazzeri, N. Marzari, and F. Mauri, Thermal Conductivity of Graphene and Graphite: Collective Excitations and Mean Free Paths, Nano Letters **14**, 6109 (2014).

[18] L. Lindsay, D. A. Broido, and N. Mingo, Flexural phonons and thermal transport in graphene, Physical Review B **82**, 115427 (2010).